JCTC Journal of Chemical Theory and Computation

pubs.acs.org/JCTC Article

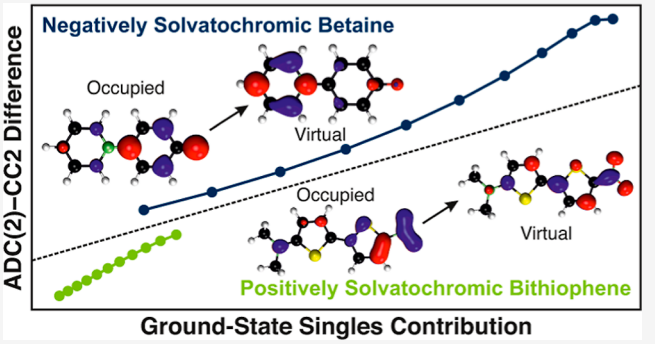
Role of Singles Amplitudes in ADC(2) and CC2 for Low-Lying Electronically Excited States

Niklas Sülzner* and Christof Hättig

Cite This: https://doi.org/10.1021/acs.jctc.3c01355 Read Online

ACCESS | Metrics & More | Article Recommendations | Supporting Information

ABSTRACT: The closely related second-order methods CC2 and ADC(2) usually perform very similarly for single excitations of organic molecules. However, as rationalized in this work, significant deviations between these two methods can arise if the ground state and a low-lying singly excited state arise from a strong coupling between their leading configurations. Such a configuration mixing is partially accounted for in CC2 through the ground-state singles amplitudes but is omitted in ADC(2). This can cause unusual deviations between the results obtained with these methods. In this work, we study how severe this effect can become at the example of two solvatochromic dyes: the negatively solvatochromic betaine dye **N1-tBu** and the positively solvatochromic bithiophene **P1**. These two dyes allow one to study the limits of both small and somewhat larger excitation energies and configuration mixing by tuning the $S_0 \rightarrow S_1$ transition energy through the polarity of the environment. Higher-level calculations at the CC3 level provide information on the accuracy of ADC(2) and CC2 in these cases. The most extreme deviation between ADC(2) and CC2 is found for **N1-tBu** in vacuum, where the ADC(2) result is 0.45 eV below that of CC2. In this case, the methodical error of CC2 with respect to CC3 is only 0.05 eV. With increasing excitation energy in polar solvents, the CC2−ADC(2) deviation decreases and reaches a value of only 0.15 eV. For **P1**, which has larger excitation energies, these effects are reversed due to the opposite solvatochromism but also smaller in magnitude: the deviation increases from 0.08 eV in vacuum to 0.16 eV in the so-called conductor limit of the continuum solvation model. Although for these two dyes larger deviations are observed for smaller excitation energies, the extent of configuration mixing does not generally correlate with only the size of excitation energy. For example, s-triazine (0.15 eV), formamide (0.19 eV), and formaldehyde (0.23 eV) also show large deviations between CC2 and ADC(2) despite their much higher excitation energies compared to those of **N1-tBu** and **P1**.



Downloaded via RUHR UNIVERSITAT BOCHUM on March 7, 2024 at 08:43:27 (UTC).
See https://pubs.acs.org/sharingguidelines for options on how to legitimately share published articles.

1. INTRODUCTION

The approximate coupled cluster singles and doubles model[1] CC2 and the closely related algebraic diagrammatic construction scheme through second order[2] ADC(2) have established as popular methods for the description of electronically excited states for single-reference molecules.[3] A beneficial compromise between good accuracy and medium computational costs [$O(N^5)$ scaling with the system size N] is what makes these two second-order methods very attractive for excitation energies (vide infra) when an accuracy beyond that of time-dependent density functional theory (TDDFT) with standard functionals is wanted. Moreover, they have also established as important methods for the optimization of excited-state geometries.[4−6]

There exists a plethora of different benchmarks for excitation energies, e.g., see ref 7 for a recent review proposing a database for highly accurate excitation energies or ref 8 for a review on 0−0 transition energies. It is known from these benchmarks that CC2 and ADC(2) perform usually very similarly for single excitations of organic molecules (see Table 1 for an overview).[9−22] This is also expected for single-reference molecules due to the similarity of the two methods. Both give energies for the ground state and for singly excited states that are correct through second order in Møller−Plesset perturbation theory (MPPT).[1,2] While ADC(2) employs for this purpose first-order ground-state double excitation amplitudes from perturbation theory, CC2 uses ground-state single and double excitation amplitudes from approximate coupled-cluster equations. However, the singles amplitudes contribute to the transition energy for singly excited states only from third order on and to the ground-state energy only starting from fourth order if the

Received: December 12, 2023
Revised: February 16, 2024
Accepted: February 16, 2024

© XXXX The Authors. Published by American Chemical Society

Table 1. Performance of ADC(2) and CC2 for 0−0 Transition and Vertical (Electronic) Excitation Energies (VEEs) for Single-Dominant Excitations as Reported in Previous Benchmarks[a]

						CC2	ADC(2)	
authors	year	ref	type	size	reference energies	ME ± SD	ME ± SD	comment
Send et al.	2011	9	0−0	15	Expt.	0.19 ± 0.26	0.14 ± 0.34	
Winter et al.	2013	10	0−0	66	Expt.	0.00 ± 0.09	−0.03 ± 0.12	
Jacquemin et al.	2015	11	0−0	80	Expt	0.03 ± 0.17	−0.03 ± 0.18	In solution (PCM)
Suellen et al.	2019	12	0−0	41	Expt	0.05 ± 0.10	−0.03 ± 0.16	Incl. 36 hybrid functionals
Sauer et al.	2008	14	VEE	121	CC3/TZVP	0.13 ± 0.26		Set from ref 13
Silva-Junior et al.	2009	15	VEE	22	CC3/aug-cc-pVTZ	0.11 ± 0.17		Incl. basis set effects
Winter and Hättig	2011	16	VEE	89	CC3/aug-cc-pVTZ	0.09 ± 0.14		Set from refs 13,14,15.
Harbach et al.	2014	17	VEE	114	CC3/aug-cc-pVTZ	0.14 ± 0.29	−0.03 ± 0.54	Set from refs 13,14,15.
Loos et al.	2018	18	VEE	106	TBE/aug-cc-pVTZ[b]	0.03 ± 0.28	−0.01 ± 0.28	Small molecules
Loos et al.	2020	19	VEE	218	TBE/aug-cc-pVTZ[c]	0.03 ± 0.20	0.01 ± 0.19	Medium-sized molecules
Loos et al.	2020	20	VEE	30	CCSDT/aug-cc-pVDZ	0.07 ± 0.14	−0.02 ± 0.17	Exotic mol. and radicals
Loos and Jacquemin	2021	21	VEE	90	TBE/aug-cc-pVTZ[b]	0.00 ± 0.15	−0.01 ± 0.13	Large molecules
Sarkar et al.	2021	22	VEE	46	TBE/aug-cc-pVTZ[c]	0.03 ± 0.29	0.02 ± 0.29	—

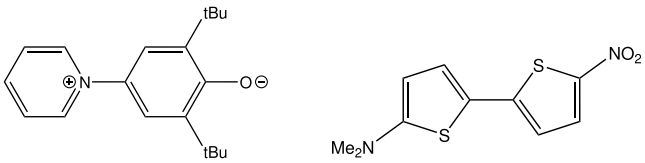
[a]Abbreviations: ME (mean error), SD (standard deviation), TBE (theoretical best estimate), and VEE (vertical excitation energy). [b]Extrapolated FCI/aug-cc-pVTZ. [c]Corrected CC3/aug-cc-pVTZ.

Hartree−Fock (HF) reference wave function fulfills the Brillouin condition.[23]

For 0−0 transition energies of the lowest valence excitations in organic closed-shell molecules, mean errors of less than 0.1 eV (in magnitude) with respect to experiments have been observed for both methods, with tendencies for CC2 to over and ADC(2) to underestimate the experimental results, respectively.[9−12] For vertical excitation energies, CC2 and ADC(2) are typically compared to higher-level reference methods such as the approximate coupled cluster singles, doubles, and triples method (CC3), revealing intrinsic methodical errors of 0.1−0.2 eV for single excitation dominated valence transitions for both CC2 and ADC(2) with respect to CC3.[13−22] For comparison, TDDFT has a typical accuracy of 0.2−0.4 eV.[12,24] In fact, CC2 typically yields for single excitations results of comparable accuracy as the more expensive [$O(N^6)$ scaling] coupled-cluster singles and doubles model (CCSD), which is additionally known to suffer from less accurate ground-state geometries due to a less fortunate error cancellation.[13,15] Further significant improvements in the accuracy of excitation energies are typically only obtained when connected triples are included, e.g., with CC3,[23,25] which comes at drastically increased computational costs [$O(N^7)$].[14,15]

However, despite the fact that CC2 and ADC(2) are both iterative methods that give for singly excited states results complete through second order MPPT, we have observed recently for the lowest excited states of some organic dyes significant differences between CC2 and ADC(2). Examples are 2,6-diphenyl-4-(2,4,6-triphenylpyridinium-1-yl) phenolate[26] (0.48 eV)—also known as betaine 30 (**B30**) or Reichardt's dye[27]—and some hydroxypyrene derivatives[28,29] (∼0.05 eV for acids and ∼0.12 eV for bases). For a simplified version of **B30**, namely, 2,6-di-*tert*-butyl-4-pyridinium phenolate (**N1-tBu**; Figure 1a), Plenert et al. reported values for the vacuum $S_0 \rightarrow S_1$ transition of 632 nm (1.96 eV) for CC2 and 830 nm (1.49 eV) for ADC(2), i.e., a difference of almost 0.5 eV.[30] In contrast, the typical deviation between CC2 and ADC(2) for excitation energies are on the order of 0.01−0.03 eV for closed-shell organic molecules.[10,11]

In refs 26 and 28 it has been hypothesized that these deviations are caused by sizable contributions of the singly excited determinants dominating the excited states to the correlated ground-state wavefunction that are not captured by the wavefunction in first order MPPT. It has been argued that in ADC(2), the omission of contributions arising from these ground-state singles amplitudes leads to excitation energies that are smaller compared to CC2 which includes the singles in the ground-state wave function.



(a) N1-tBu (b) P1

Figure 1. Molecular structures of the dyes studied here: (a) 2,6-di-*tert*-butyl-4-pyridinium phenolate (**N1-tBu**) and (b) 5-(dimethylamino)-5′-nitro-2,2′-bithiophene (**P1**).

The purpose of this article is to shed some light on the origins and consequences of this difference between CC2 and ADC(2) for excited states and validate the above hypothesis. In particular, we aim to investigate how large or severe this effect from the singles amplitudes can become by investigating typical cases, both in the regions of very small and less small excitation energies. To illustrate this, we will use two dye molecules (Figure 1), the negatively solvatochromic dye **N1-tBu** and the positively solvatochromic dye **P1**, with a focus on their lowest excited states. Due to the solvatochromism of these dyes, a polarizable continuum environment can be used to tune the magnitude of the effect via the $S_0 \rightarrow S_1$ transition energy without changing the molecule and the electronic structure of the involved states. In the following, we will first present a brief description of the theoretical background that is helpful for understanding the influence of the singles amplitudes for ADC(2) and CC2.

2. THEORETICAL BACKGROUND

2.1. Approximate Coupled Cluster Models CC*n*. CC2 and CC3 are two examples of approximate coupled cluster models that belong to the CC*n* family of methods which have been specifically designed for response calculations.[1,23] In general, a CC*n* method is derived from a coupled cluster

https://doi.org/10.1021/acs.jctc.3c01355
J. Chem. Theory Comput. XXXX, XXX, XXX−XXX

(CC) method truncated at an excitation level n by approximating the n-tuple cluster equations. The idea is to keep only those terms in the latter equations that enter in lowest nonvanishing order (in MPPT). The singles are counted thereby as being of zeroth order, i.e., they are not approximated because of their importance for response properties and excitations energies.

For example, CC2 is derived from CCSD, whose (ground-state) amplitude equations are given by

$$\langle \mu_1 | \hat{\bar{H}} + [\hat{\bar{H}}, \hat{T}_2] | \mathrm{HF} \rangle = 0 \tag{1}$$

$$\left\langle \mu_2 \middle| \hat{\bar{H}} + [\hat{\bar{H}}, \hat{T}_2] + \frac{1}{2}[[\hat{\bar{H}}, \hat{T}_2], \hat{T}_2] \middle| \mathrm{HF} \right\rangle = 0 \tag{2}$$

where $\hat{\bar{H}} = \exp(-\hat{T}_1)\hat{H}\exp(\hat{T}_1)$ denotes the Hamiltonian that is similarity-transformed with the single excitation part, $\hat{T}_1$, of the cluster operator. $\hat{T}_2$ is the corresponding double excitation part, $|\mathrm{HF}\rangle$ the HF reference wave function, and μ_1 and μ_2 denote, respectively, singly and doubly excited determinants (for further details on CC theory see, e.g., refs 31−33).

In the CC2 model, the singles equations are kept unchanged, while the doubles equations of CCSD are simplified such that they contain only terms to lowest nonvanishing (i.e., first) order.[1] Introducing the standard partitioning of the Hamiltonian $\hat{H} = \hat{F} + \hat{U}$ into a Fock operator $\hat{F}$ and a fluctuation potential $\hat{U}$, the doubles equations for CC2 finally become

$$\langle \mu_2 | [\hat{F}, \hat{T}_2] + \hat{\bar{H}} | \mathrm{HF} \rangle = 0 \tag{3}$$

The CC2 ground-state energy is of MP2 quality and does not provide a significant improvement beyond MP2. However, unlike MP2, CC2 allows to describe excited-states and their properties within the framework of response theory (vide infra).

2.2. Relation between ADC(2) and CC2. In response theory, electronic excitation energies are obtained as eigenvalues ω_k of a stability matrix (cf. eq 4). For a review on excited-state CC methods, see, e.g., ref 34. For variational methods, the stability matrix is the electronic Hessian and for nonvariational methods like CC2 the electronic Jacobian **A**.

$$(\mathbf{A} - \omega_k \mathbf{S})\vec{R}^{(k)} = 0 \tag{4}$$

In the last equation, **S** is the metric in the space of the wavefunction parameters and $\vec{R}^{(k)}$ the right eigenvector for the eigenvalue ω_k. For CC2, the Jacobian contains all contributions that are needed to obtain excitation energies for single-excitation dominated transitions correct through second order in the fluctuation potential, while the energies for double excitations are only correct through zeroth order.[1] A detailed analysis exploring in which order MPPT different terms in the Jacobian contribute to excitation energies can be found in ref 35.

A second-order method closely related to CC2 is ADC(2), the algebraic diagrammatic construction scheme (for the polarization propagator) through second order. ADC(2) is not based on linear response theory of a corresponding ground-state method, but derived within the polarization propagator approach.[2] Despite their different origins, an analysis of the structure of the respective secular matrices from which the excitation energies are obtained allows to identify the similarities between ADC(2) and CC2 from a more pragmatic, technical perspective.[4] Accordingly, if we consider the CC2 Jacobian, $\mathbf{A}^{\mathrm{CC2}}$, as a function of the ground-state singles (T_1) and doubles (T_2) amplitudes, i.e.,

$$\mathbf{A}^{\mathrm{CC2}} = \mathbf{A}^{\mathrm{CC2}}(T_1, T_2), \tag{5}$$

then, the ADC(2) secular matrix, $\mathbf{A}^{\mathrm{ADC(2)}}$, is identical with the Hermitian part of a CC2-like Jacobian calculated with the first-order amplitudes

$$\mathbf{A}^{\mathrm{ADC(2)}} = \frac{1}{2}(\mathbf{A}^{\mathrm{CC2}}(0, T_2^{(1)}) + \mathbf{A}^{\mathrm{CC2}}(0, T_2^{(1)\dagger})) \tag{6}$$

(Note that we assume here a closed-shell or spin-unrestricted HF reference).

Equation 6 reveals two important differences between ADC(2) and CC2. First, the CC2 cluster amplitudes are replaced by those from first-order MPPT, i.e., the singles T_1 are neglected and T_2 is approximated by $T_2^{(1)}$. Second, the ADC(2) secular matrix is Hermitian. The hermiticity of the secular matrix is important for a qualitatively correct description of conical intersections (CI) between two excited states,[4] but should not significantly affect excitation energies outside a region where the respective state is involved in a CI. In fact, the matrix $\mathbf{A}^{\mathrm{CC2}}(0, T_2^{(1)})$ in eq 6, i.e., the one that also includes the non-Hermitian part, is identical to the secular matrix of $\mathrm{CIS}(\mathrm{D}_\infty)$.[36] The latter method is known to yield excitation energies that are very close to those of ADC(2).[4] The neglect of the ground-state singles in ADC(2) has, to the best of our knowledge, in the literature up to now not been considered to be important. However, a closer inspection shows that T_1 allows for a coupling between the ground and singly excited states in the sense that the configuration state functions that dominate these states can contribute to both, the ground and the excited states, if they belong to the same spin and symmetry. For CC methods, the ground and excited ket states are obtained as[37]

$$|0\rangle = |\mathrm{CC}\rangle = \exp(\hat{T})|\mathrm{HF}\rangle = (1 + \hat{T}_1 + \frac{1}{2}\hat{T}_1^2 + \hat{T}_2 + \ldots)|\mathrm{HF}\rangle \tag{7}$$

$$\begin{aligned} |k\rangle &= (s^{(k)} + \hat{R}^{(k)})|\mathrm{CC}\rangle \\ &= (s^{(k)} + \hat{R}_1^{(k)} + s^{(k)}\hat{T}_1 + \hat{R}_1^{(k)}\hat{T}_1 + \hat{R}_2^{(k)} + \ldots)|\mathrm{HF}\rangle \end{aligned} \tag{8}$$

where $\hat{R}^{(k)}$ is the excitation operator build with the elements of the eigenvector $\vec{R}^{(k)}$ and

$$\begin{aligned} s^{(k)} &= \omega_k^{-1}\langle \mathrm{HF}|[\hat{\bar{H}}, \hat{R}^{(k)}]|\mathrm{HF}\rangle \\ &= \omega_k^{-1}\langle \mathrm{HF}|\hat{\bar{H}}(\hat{R}_1^{(k)}\hat{T}_1 + \hat{R}_2^{(k)})|\mathrm{HF}\rangle \end{aligned} \tag{9}$$

is the coefficient of the reference state in the ket wavefunction for the excited state k. If state k has the same spin and symmetry as the ground state, $s^{(k)} \neq 0$ and $\vec{R}^{(k)}$ is not orthogonal to the ground-state amplitude vector, i.e., $|\mathrm{HF}\rangle$ can contribute to $|k\rangle$ and an excited configuration dominating $|k\rangle$ can contribute to $|0\rangle$. Including this configuration mixing will lower the energy of the lower (ground) state and increase the energy of the higher (excited) state compared to results obtained with wavefunctions that omit such mixing. The latter is the case for (purely) singly excited states when T_1 is not included and thus $\vec{R}^{(k)}$ is orthogonal to the ground-state amplitude vector and $s^{(k)} = 0$.

https://doi.org/10.1021/acs.jctc.3c01355
J. Chem. Theory Comput. XXXX, XXX, XXX−XXX

2.3. Designing a Challenge for Second-Order Methods. Stimulated by the cases with large deviations between ADC(2) and CC2 mentioned in the introduction, the following question is of central interest: when is it expected that the ground-state singles amplitudes can make a significant contribution to excitation energies? Pursuing the previous considerations, this can only be the case if the ground and a low-lying excited state have the same symmetry (i.e., belong to the same irreducible representation) and if both states have characters where two configurations—corresponding to different Lewis structures—one dominating the ground and one the excited state, can mix. Based on these reasons, important examples of this situation are solvatochromic dyes: they have low-lying excited states with a polarity strongly different from that of the ground states so that one of them is stabilized and the other is destabilized in polar solvents. If the ground state S_0 is more polar than the first excited state S_1, the $S_0 \rightarrow S_1$ transition energy increases with increasing polarity of the solvent due to a stronger stabilization of S_0 compared to S_1. This is termed negative solvatochromism. Inversely, positive solvatochromism refers to a decrease of the $S_0 \rightarrow S_1$ transition energy with increasing solvent polarity owing to S_1 being more polar, and thus more strongly stabilized, compared to S_0. Therefore, we have studied two main examples, one for each type of solvatochromism.

2.3.1. First Example: A Negatively Solvatochromic Dye. As the first example, we selected 2,6-di-*tert*-butyl-4-pyridinium phenolate (**N1-tBu**): a smaller—and therefore computationally more friendly—model for the prominent **B30**, recently suggested by Plenert et al.[30] **N1-tBu** inherits the same pronounced negative solvatochromism from its parent **B30**, although the solvatochromic window (chloroform → water) is slightly smaller for **N1-tBu** (0.85 eV, 6900 cm^{-1}) compared to **B30** (1.04 eV, 8400 cm^{-1}).[30] In details, the $S_0 \rightarrow S_1$ absorption of **N1-tBu** undergoes a blueshift from 618 nm (16,200 cm^{-1}) in chloroform to 433 nm (23,100 cm^{-1}) in water.[30] The idea behind this choice is to have a molecule with a (very) small S_0–S_1 energy gap in the gas phase, where singles contributions become important, and a larger gap in a polar environment.

2.3.2. Second Example: A Positively Solvatochromic Dye. As the second example, we have selected the dye 5-(dimethylamino)-5′-nitro-2,2′-bithiophene (**P1**) from Reichardt's table of solvatochromic compounds,[27] chosen as a compromise between a large solvatochromic window (4710 cm^{-1}), a still comparably low transition energy [<3 eV (24,000 cm^{-1})], and feasible computational costs (system size). The $S_0 \rightarrow S_1$ absorption of **P1** undergoes a red shift from 466 nm (21,460 cm^{-1}) in hexane to 597 nm (16,750 cm^{-1}) in formamide/water.[38,39] Most typical positively solvatochromic dyes have either larger transition energies (>3 eV) or small to moderate solvatochromic windows.[27] However, with **P1**, we further extend the range of transition energies spanned together with **N1-tBu**.

2.4. Utilizing COSMO for Tuning the State Mixing. These two dyes allow the extent of coupling between S_0 and S_1 to be changed by varying the polarity of the environment. While, in principle, any field (e.g., an arbitrary external electric field) could be used for this purpose, we employ for convenience the reaction field (RF) from the conductor-like screening model (COSMO).[40−42] COSMO, which belongs to the family of dielectric continuum solvation models,[43] treats the solute as being located in a molecularly shaped cavity that is surrounded by the solvent depicted as a structure-less dielectric medium with basically just a single property, i.e., its (relative) electric permittivity ϵ_r (often simply referred to as dielectric constant). Only purely electrostatic solute−solvent interactions via mutual polarization of the solute and the embedding dielectric continuum are considered. For the latter, COSMO introduces a conductor-like approximation by using a scaled conductor boundary condition instead of the more complicated, exact dielectric boundary condition.[40] The scaling factor is defined as

$$f(\epsilon_r) = \frac{\epsilon_r - 1}{\epsilon_r + x} \tag{10}$$

where $x = 0.5$ is used in COSMO.[40,44] The scaling function is $f(\epsilon_r) = 0$ in the vacuum limit, where $\epsilon_r = 1$, and increases monotonically with increasing dielectric constant until $f(\epsilon_r) = 1$ in the so-called conductor limit,[40] $\epsilon_r = \infty$.

Since the solute and the solvent mutually polarize each other, the Schrödinger equation for the wavefunction of the solute becomes nonlinear. While this is straightforwardly accounted for in self-consistent-field (SCF) methods like HF by updating the screening charges during the SCF steps,[45] this requires more attention for post-HF methods, including CC methods.[46,47] We do here not aim at an accurate modeling of the excitation energies in solution, but merely use the implicit solvent model as a mean for tuning the $S_0 \rightarrow S_1$ energy gap through $f(\epsilon_r)$. Therefore, we use below the computationally efficient and simple perturbation through the energy[48,49] (PTE) and post-SCF[50,51] coupling schemes that are available for ADC(2) and CC2.

In the PTE scheme,[48,49] the correlation and excitation energies are evaluated with the molecular orbitals (MOs) and the electrostatic potential caused by the environment, without including further contributions to the mutual polarization of the environment and the solute. The post-SCF scheme[50,51] additionally includes for CC2 in the ground-state equations a correlation contribution to the environment potential arising from T_1. For both ADC(2) and CC2, the post-SCF scheme does for the excitation energy include the linear-response (LR) but no state-specific contributions. In dielectric continuum solvation models like COSMO, the square of the refractive index replaces the static dielectric constant in the linear response contributions from the environment according to $f(\epsilon_r) \rightarrow f(n^2)$. These LR contributions always lower the excitation energies. However, they only affect the transitions between the ground and the excited states, i.e., the excitation energies and eigenvectors, but not the ground-state wavefunction itself. Therefore, this work focuses on the variation of $f(\epsilon_r)$.

3. COMPUTATIONAL DETAILS

All calculations except those with CC3 have been done using version 7.7 of the TURBOMOLE program package,[52,53] while a development version of the ccsdf12 module[54] has been used for CC3. The resolution-of-the-identity (RI) approximation has been employed in the DFT calculations for the geometry optimizations (modules[55,56] ridft and rdgrad) and in the ADC(2), CC2, and CC3 calculations of excitation energies (modules ricc2 and ccsdf12). Additionally, the frozen-core approximation has been applied for the electrons in the 1s orbitals at C, N, and O and the 1s2s2p orbitals at S. To ensure convergence with diffuse basis functions, the integral screening threshold for the MO calculations ($scftol) was lowered to 10^{-15}. Environmental effects through polarization in solution were accounted for via the implicit solvent model COSMO.

https://doi.org/10.1021/acs.jctc.3c01355
J. Chem. Theory Comput. XXXX, XXX, XXX−XXX

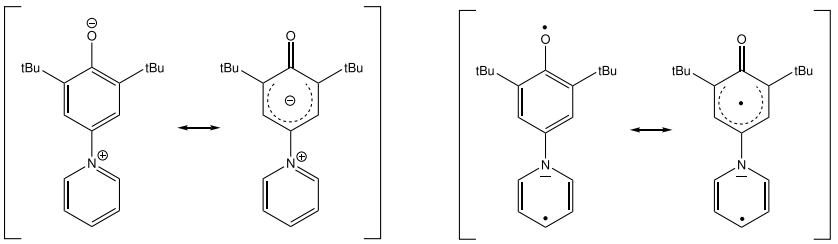
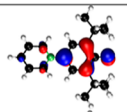
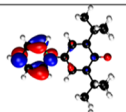
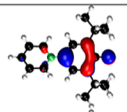
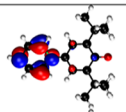
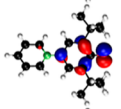
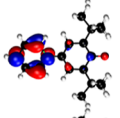
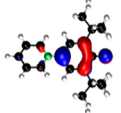
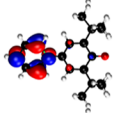
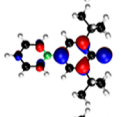
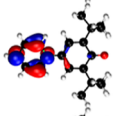
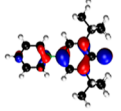
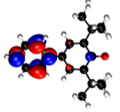
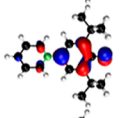
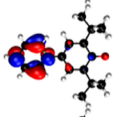
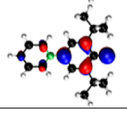
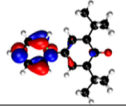


Figure 2. Lewis resonance structures of **N1-tBu** contributing to its singlet ground state (a) and first excited state (b) (note that in S_1 one unpaired electron is delocalized in the phenolate moiety and one is delocalized in the pyridine ring).

Table 2. Overview on the Dominating NTO Pair for the First Electronic Transition with ADC(2) and CC2 as Well as for the CC2 and CC3 Ground-State Singles Amplitudes of Dye N1-tBu in Vacuum (Left) and in the Conductor Limit (Right)[a]

		Vacuum			Conductor Limit		
Method	State	Occ. NTO	Vir. NTO	Weight (D_1)	Occ. NTO	Vir. NTO	Weight (D_1)
ADC(2)	S_1			98.6 %			99.1 %
CC2	S_1			99.0 %			99.2 %
CC2	S_0			61.2 % (0.19)			52.7 % (0.17)
CC3	S_1			97.9 %	—	—	—
CC3	S_0			59.7 % (0.16)	—	—	—

[a]NTO weights and, for the ground-state, D_1 diagnostics are also included.

Default parameters were used for the cavity construction. All molecular structures together with their HF or DFT energies are available in a data publication on Zenodo.[57]

Ground-state equilibrium geometries have been optimized in the gas phase using DFT with the B3-LYP[58−60] functional for RI-DFT[55,56,61] in the def2-TZVP[62] basis set with the m4 grid.[56,61] At these geometries, vertical electronic excitation energies and oscillator strengths have been calculated in the aug-cc-pVDZ[63,64] basis set with ADC(2) and CC2 for the gas phase and COSMO-ADC(2)[51] and COSMO-CC2[51] in polar environments. For excitation energies in the gas phase (vacuum), CC3 calculations have also been carried out. Some of the CC3 calculations for **N1-tBu** have been done in a restricted virtual space (RVS) with a cutoff of 2 E_h (54.42 eV), introducing a shift in the excitation energy of ca. 0.02 eV at the CC2 level. Furthermore, for a theoretical best estimate (TBE) of the vacuum excitation energy of **N1-tBu**, the geometry has been reoptimized for C_2 symmetry with CC2[65] in the cc-pVTZ[66] basis set. At this geometry, the excitation energies have been calculated with CC2 in the aug-cc-pVXZ basis sets with X = D, T, Q, 5[63,67] and with CC3 in the aug-cc-pVDZ[63] basis set. Ground and excited-state dipole moments (μ) mentioned in the text refer to orbital-relaxed CC2 results in the gas phase. For the combination of COSMO with the methods ADC(2) and CC2 for excited states, the post-SCF coupling scheme (non-equilibrium limit) has been used. For additional comparison in the case of **N1-tBu**, the PTE coupling scheme has also been used, which neglects LR contributions. To generally switch off the LR contributions and selectively probe the effect on the excitation energies through the ground-state RF, a refractive index of $n = 1$ has been used, unless stated differently. Note that PTE and post-SCF are identical for ADC(2) in the special case of $n = 1$.

For the visualization of electronic transitions, natural transition orbitals (NTOs) are used.[68−70] For the excited states, they are obtained from a singular value decomposition (SVD) of the singles part of the eigenvectors for the states k, arranged for this purpose in a matrix $\mathbf{R}_1^{(k)}$

$$\mathbf{R}_1^{(k)} = \sum_j \sigma_j^{(k)} \vec{u}_j^{(k)} \vec{v}_j^{(k)} \tag{11}$$

The normalized singular vectors $\vec{u}_j^{(k)}$ and $\vec{v}_j^{(k)}$ correspond to coefficient vectors for occupied (hole) and virtual (particle) orbitals for individual orbital transitions, while the singular values $\sigma_j^{(k)} > 0$ carry the information on the importance of their

https://doi.org/10.1021/acs.jctc.3c01355
J. Chem. Theory Comput. XXXX, XXX, XXX−XXX

contribution to $\mathbf{R}_1^{(k)}$. The relative NTO weights reported below are defined as $w_i^{(k)} = \sigma_j^{(k)}/\sum_j \sigma_j^{(k)}$.

In analogy to the single-excitation part of the eigenvectors, SVD can also be applied to analyze the ground-state singles amplitudes T_1. This is directly related to the D_1 diagnostic proposed by Janssen and Nielsen to quantify correlation effects in the ground state that originate from a mixing with singly excited configurations.[71] For CC and MPPT methods, this diagnostic is defined as the 2-norm or largest singular value of the matrix containing the ground-state singles amplitudes

$$D_1 = \|T_1\|_2 = \sigma_{\max} \tag{12}$$

For MP2, D_1 is calculated from the second-order singles amplitudes.[71] A large value of D_1 indicates a multireference character of the ground state due to a large contribution from a singly excited configuration.

Similar to the excited states, we can interpret the singular vectors as coefficients for NTOs. They describe in this case the change from the HF to the singles part of the correlated wavefunction. Due to the intermediate normalization of the CC wave function, the singular values have in this case the meaning of coefficients of the respective singly excited determinant in $|CC\rangle$. Weights of 99.0% for S_1 or 61.2% for T_1 in CC2 mean that the corresponding NTO pairs contribute with these fractions to the CC2 excitation vector or ground-state singles amplitudes, respectively.

4. RESULTS

4.1. Example of Negative Solvatochromism. *4.1.1. Effect of the Ground-State Reaction Field.* For betaine **N1-tBu**, as an example of a negatively solvatochromic dye, the electronic ground state, S_0, is more polar (μ = 8.6 D) compared to the electronically first excited state, S_1 (μ = 5.1 D). This can be also rationalized based on Lewis resonance structures for the two states (Figure 2): the closed-shell nature of the ground-state of **N1-tBu** requires a charge separation in S_0, leading to a zwitterionic character with partial negative and positive charges at the O and N atoms, respectively. Upon excitation to the diradicalic S_1 state, a charge transfer takes place, as seen from the NTOs in Table 2. This partially cancels the charge separation and reduces the dipole moment. The zwitterionic configuration of the ground state is less favorable in vacuum than in a polar environment. Therefore, the energy difference between S_0 and S_1 is relatively small in vacuum (ϵ_r = 1), based on the calculated vertical $S_0 \rightarrow S_1$ transition energies of 1.55 and 2.00 eV for ADC(2) and CC2, respectively (Table 3). The difference of 0.45 eV between ADC(2) and CC2 is significantly larger than what is typically observed for $\pi \rightarrow \pi^*$ single excitations of organic molecules (cf. Table 1). CIS(D_∞) yields an excitation energy of 1.55 eV that is identical with the ADC(2) result. This shows that the difference between ADC(2) and CC2 observed here originates from the contributions of T_1 to the CC2 Jacobian and not from the missing hermiticity. This difference can be traced back to a configuration interaction between S_0 and S_1: if both electronic states belong to the same irreducible representation, a mixing of the contributions to the wavefunction is observed for CC2. The same NTO pair that is dominating the $S_0 \rightarrow S_1$ transition also has a significant contribution to the ground state through the singles (T_1) amplitudes (see left part of Table 2). This mixing is absent for ADC(2) whose ground state is described by an MP1 wave function without singles, hence yielding a significantly smaller excitation energy compared to CC2. The absence of the contribution from T_1 in the MP1 amplitudes and thus the lack of mixing between the zwitterionic and neutral configurations are in line with a slightly larger ground-state dipole moment for MP2 (9.3 D) than for CC2 (8.6 D).

In polar solvents, the more polar S_0 state of **N1-tBu** is stabilized more strongly compared to the less polar S_1 state and hence the $S_0 \rightarrow S_1$ transition energy increases from vacuum to the conductor limit by ca. 0.73 eV for ADC(2), but only by ca. 0.25 eV for CC2 (Table 3). When the polarity of the environment is increased from the vacuum [ϵ_r = 1 and $f(\epsilon_r)$ = 0] to the conductor limit [$\epsilon_r = \infty$ and $f(\epsilon_r)$ = 1], we can observe that (cf. Figure 3):

(i) the $S_0 \rightarrow S_1$ excitation energy becomes larger,
(ii) the NTO pair for the $S_0 \rightarrow S_1$ transition contributes less to the CC2 ground state, and
(iii) the difference between CC2 and ADC(2) becomes significantly smaller (−0.025 eV) than in vacuum, reaching a value that is typical for low-lying $\pi \rightarrow \pi^*$ single excitations of organic molecules.

Table 3. First Vertical Electronic Excitation Energies in eV for N1-tBu with ADC(2) and CC2 in Combination with COSMO for Different Media

ϵ_r	n	medium	ADC(2)	CC2	diff.
1	1	vacuum[c]	1.550	2.000	+0.450
1.43	1.265	solid Ar[a]	1.501	1.823	+0.322
1.52	1.360	solid Kr[a]	1.487	1.769	+0.282
1.71	1.477	solid Xe[a]	1.487	1.711	+0.224
1	∞	[d]	1.127	1.273	+0.146
∞	1	conductor limit[c]	2.272	2.247	−0.025
46.45	1.479	DMSO[b]	2.124	2.005	−0.119

[a]Exptl. λ_{max} (ref 30): 1.805 eV (Ar), 1.802 (Kr), 1.797 eV (Xe). [b]Exptl. λ_{max} (ref 30): 2.234 eV. [c]Without LR contributions. [d]Only LR contributions, $f(n^2)$ = 1.

4.1.2. State Mixing in the First Transition. A comparison of ADC(2) and CC2 over the range of $f(\epsilon_r)$ allows monitoring of how the deviation between these two methods changes with the S_0−S_1 energy gap from the vacuum to the conductor limit. For ADC(2) as well as CC2, the $S_0 \rightarrow S_1$ vertical excitation energies with the PTE coupling scheme show a continuous increase with $f(\epsilon_r)$ (see Figure 3a). Concomitantly, both the D_1(MP2) and the D_1(CC2) diagnostics, describing a mixing of the ground-state with singly excited configurations,[71] decrease continuously with $f(\epsilon_r)$, in particular D_1(MP2) decreases almost linearly (cf. Figure 3b). In contrast, for CC2, the results with the PTE and post-SCF coupling scheme differ. While the differences in the excitation energy point toward post-SCF contributions to the ground-state RF that lower the excitation energy, the more complicated and almost parabolic progression of the D_1(CC2) or the related weight of the dominant T_1 NTO pair might be related to the nonlinearity of the CC2 amplitude equations. Overall, these results indicate that for **N1-tBu** singly excited determinants contribute the less the larger the $S_0 \rightarrow S_1$ transition energy is.

Furthermore, over the range from 0.0 to 0.3 for $f(\epsilon_r)$, CC2 also shows a significant mixing between the lowest-lying $\pi \rightarrow \pi^*$ and the lowest-lying $n \rightarrow \pi^*$ transitions that is absent in ADC(2), as can been seen by changes in the NTOs (Tables S1 and S2, Supporting Information) or the oscillator strengths (Figure S1). In the vacuum limit, $f(\epsilon_r)$ = 0.0, where this mixing is strongest,

https://doi.org/10.1021/acs.jctc.3c01355
J. Chem. Theory Comput. XXXX, XXX, XXX−XXX

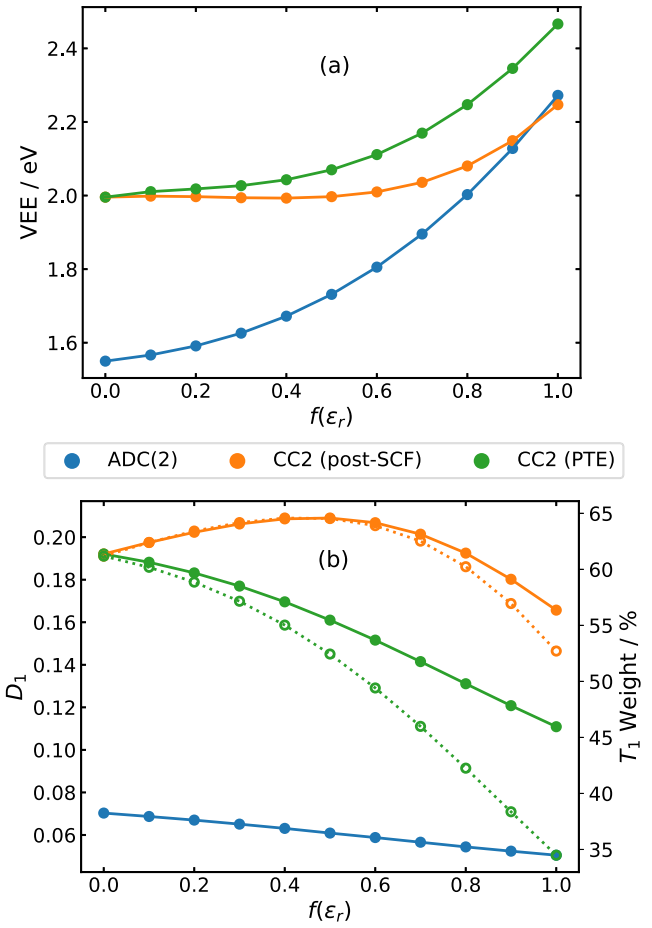


Figure 3. Variation of the ADC(2) and CC2 first vertical excitation energies in (a) and D_1 diagnostic values (solid lines, dots) and ground-state T_1 amplitude NTO weights (dashed lines, circles) in (b) with electric permittivity for **N1-tBu** in vacuum.

the occupied parts of the dominant NTOs for S_1 and S_2 with CC2 involve both a combination of $n\pi^*$ and $\pi\pi^*$ contributions from the aromatic system, which are located within or perpendicular to the ring plane, respectively. These $n\pi^*$ and $\pi\pi^*$ contributions further overlap with either of the 2p orbitals at the O atom. As the polarity increases, the $\pi\pi^*$ contribution intensifies while the $n\pi^*$ contribution diminishes for S_1, maximizing overlap with a 2p orbital at the O atom perpendicular to the plane and thus yielding $\pi\pi^*$ character for the S_1 state (cf. Table S1). Vice versa, S_2 becomes a pure $n\pi^*$ excited state with the occupied NTO dominated by one of the 2p orbitals at the O atom that is located in the molecular plane.

Another manifestation of the mixing between the $\pi\pi^*$ and $n\pi^*$ states is found in the $S_0 \rightarrow S_1$ transition energy: for CC2, it remains almost constant over the range from $f(\epsilon_r) = 0.0$ to $f(\epsilon_r) = 0.5$, then slowly starts to rise, but less steeply compared to ADC(2), and finally reaches a similar value as for ADC(2) at $f(\epsilon_r) = 1.0$. Importantly, the character of the dominant NTO pair for the CC2 T_1 amplitudes remains the same over the full range of $f(\epsilon_r)$ (Table S3) and continues to resemble the NTOs for the $S_0 \rightarrow S_1$ transition with ADC(2). The latter observation is in line with the lack of $\pi\pi^*/n\pi^*$ mixing for ADC(2) since the involved T_1 contributions are missing.

This state mixing is possible because of the twisted ground-state geometry (twist angle: ~30°) which breaks the n/π separation: for a coplanar structure with C_{2v} symmetry, the $\pi\pi^*$ state belongs to the A_1 and the $n\pi^*$ state to the A_2 irreducible representations. Both states become totally symmetric for a twisted structure with C_2 point group symmetry. With decreasing mixing, e.g., with higher $f(\epsilon_r)$, the $\pi \rightarrow \pi^*$ character of the S_1 state increases, which then intensifies the interaction with S_0. For both **N1-tBu** and the model **N1**, obtained via substitution of the two computationally demanding *tert*-butyl groups by H atoms, we verified via NTO analysis (Tables S4–S7) that the mixing of the two lowest-lying electronically excited states can be avoided by forcing the two ring systems into the coplanar geometry that is only ~7 kJ mol^{-1} higher in energy. Upon planarization, the excitation energy into the $\pi\pi^*$ state increases by ca. 0.25 eV, for both **N1** and **N1-tBu** with ADC(2) as well as CC2, while that for the $n\pi^*$ state increases by ca. 0.07 eV.

4.1.3. Addressing the Accuracy of ADC(2) and CC2. To test whether ADC(2) or CC2 is more accurate when ground and singly excited states are partially mixed, we have compared them for the gas phase to the higher-level CC3 method. The gas phase is in this case also the limit where the mixing is strongest. CC3 has for ground states an accuracy comparable to that of CCSD(T) and is for singly excited states correct through third order MPPT.[23] That the lowest totally symmetric excited state has the same character with the different methods has been verified based on the NTOs. For the model system **N1**, the error of CC2 (2.157 eV) with respect to CC3 (2.122 eV) is found to be ~0.04 eV in the gas phase (Table S8), which is much smaller than the corresponding error of ~0.17 eV for ADC(2) (1.948 eV). Owing to the larger size, the CC3 calculation for **N1-tBu** has been first limited to the planar structure (C_{2v} symmetry) due to lower computational costs. For the planarized **N1-tBu**, an error of 0.04 eV for CC2 (2.269 eV) with respect to CC3 (2.229 eV) is observed, while ADC(2) (1.801 eV) differs by ~0.43 eV from CC3 (Table 4). In the course of determining a theoretical best estimate (TBE) for the vacuum excitation energy of **N1-tBu**

Table 4. Lowest Totally Symmetric Electronic Transition of N1-tBu at a Planar Geometry with ADC(2), CC2, and CC3 in Vacuum[a]

Method	VEE / eV	Occ. NTO	Vir. NTO
ADC(2)	1.801		
CC2	2.269		
CC3	2.229		

[a]All NTO weights exceed 97%.

https://doi.org/10.1021/acs.jctc.3c01355
J. Chem. Theory Comput. XXXX, XXX, XXX−XXX

(cf. Section 4.1.4), the CC3 calculation has also been repeated at a reoptimized CC2/cc-pVTZ geometry with C_2 symmetry with a restricted virtual space (RVS) to reduce the computational costs. The effect of the RVS on the excitation energy is only small here (ca. 0.02 eV for CC2), even smaller than found for other chromophores[72] and depends only weakly on the electronic structure method, i.e., has almost the same value for CC2 and CC3. For **N1-tBu** with C_2 symmetry, CC2 (1.860 eV) deviates from CC3 (2.000 eV) with ∼0.14 eV significantly less than ADC(2) (1.427 eV) does with ∼0.57 eV. The fact that CC2, and not ADC(2), is closer to CC3 demonstrates that CC2, which includes the singles in the ground-state wavefunction, yields more accurate results for **N1-tBu** (and **N1**).

4.1.4. Accurate Estimate for the Vacuum Excitation Energy. In ref 30, Plenert et al. use an extrapolation of E_T, i.e., the vertical excitation energy (expressed in kcal mol^{-1}) as a function of the normalized solvent polarity function E_T^N, to estimate the gas phase $S_0 \rightarrow S_1$ transition energy of **N1-tBu**. Using a value of $E_T^N = -0.111$ for the gas phase (as previously determined for **B30**),[73] they obtain an extrapolated value of 773 nm (1.60 eV) that disagrees with their results from TDDFT as well as those from ADC(2) (1.49 eV) and CC2 (1.96 eV). However, this extrapolation neglects effects from the refractive index of the solvent, as it solely focuses on its polarity. Since the refractive index enters through the LR contributions that always lower the excitation energy in a dielectric environment (cf. Figures S2 and S4), such an extrapolation yields presumably too small results. In fact, we obtain with CC2—without reoptimization of the vacuum geometries—excitation energies of 1.96 eV (Ar), 1.77 eV (Kr), and 1.71 eV (Xe) that only differ by −0.02, 0.03, and 0.09 eV from the experimental results in rare gas matrices,[30] respectively (cf. Table 3). To determine the vacuum excitation energy with high accuracy, we have improved the initial CC2 result (2.00 eV) by

(i) switching to a more accurate CC2/cc-pVTZ geometry (C_2 symmetry),

(ii) estimating the remaining basis set error using CC2 calculations in the aug-cc-pVXZ basis sets up to $X = 5$, and

(iii) adding to the CC3 result the correction calculated at the CC2 level for the improved geometry and the enlarged basis set (including the correction for the virtual MOs skipped in RVS approximation) (cf. Table S9).

Following this recipe, we obtain a TBE of 1.97 eV that contradicts the extrapolated result (1.60 eV). The remaining correlation error of CC3 is only about 0.02 eV for single excitations with $\pi \rightarrow \pi^*$ character,[7] meaning that in vacuum, the overall error should be dominated by the difference between the vertical electronic excitation and the maximum of the absorption band, typically[74] about −0.1 eV. A value of 1.87−1.97 eV for the band maximum in vacuum is also in line with the expectation that the excitation energies in vacuum should be slightly larger than in rare gas matrices (∼1.8 eV, cf. Table 3) where the optical polarizability is larger than its static counterpart ($n^2 > \epsilon_r$). Regarding this high level of theory, we thus anticipate that the extrapolated experimental result is too inaccurate to serve as a benchmark for calculations.

4.2. Example of Positive Solvatochromism. The bithiophene **P1**, as an example of a positively solvatochromic dye, exhibits a less polar S_0 state (μ = 9.9 D) and a more polar S_1 state (μ = 20.6 D), and hence the $S_0 \rightarrow S_1$ transition energy decreases with increasing solvent polarity (ϵ_r) (Table 5 and Figure 5a). The Lewis resonance structures for the ground state (Figure 4a) illustrate the push−pull interaction between the dimethylamino group as the donor and the nitro group as the acceptor. The structure on the left in Figure 4a should prevail for S_0. Upon excitation to S_1 (Figure 4b), a charge redistribution from the donor to the acceptor part takes place, as is visible in the NTOs (Table 6). This charge transfer intensifies the charge separation and leads to a larger dipole moment.

Table 5. First Vertical Electronic Excitation Energies in eV for P1 with ADC(2) and CC2 in Combination with COSMO for Different Media

ϵ_r	n	medium	ADC(2)	CC2	diff.
1	1	vacuum[a,c]	2.849	2.930	0.081
1	∞	[d]	2.539	2.555	0.014
∞	1	conductor Limit[c]	2.347	2.509	0.162
46.45	1.479	DMSO[b]	2.236	2.356	0.120

[a]Vacuum CC3:3.006 eV. [b]Exptl. λ_{max}: 2.201 eV (taken from ref 39). [c]Without LR contributions. [d]Only LR contributions, $f(n^2) = 1$.

We observe for **P1** that the vacuum ADC(2) (2.85 eV) and CC2 (2.93 eV) excitation energies are quite similar, differing by only 0.08 eV, a value that is typical for low-lying $\pi\pi^*$ singly excited states of organic molecules (cf. Table 1). Inversely to the negatively solvatochromic **N1-tBu**, the positively solvatochromic **P1** shows a stronger stabilization of the more polar S_1 state when placed in a polar environment compared to the less polar S_0 state: the transition energy decreases from the vacuum to the conductor limit by ca. 0.50 eV for ADC(2) and ca. 0.42 eV for CC2. Since S_0 and S_1 belong to the same irreproducible representation, their leading configurations can mix. This interaction between the ground- and excited-state configurations increases with decreasing gap in a polar environment: Both the D_1 diagnostic and the weight of the dominant NTO pair of T_1 (Figure 5b) as well as the ADC(2)−CC2 difference for the excitation energies (Figure 5a) increase with increasing $f(\epsilon_r)$. As verified by NTO analysis, this interaction appears less severe compared to **N1-tBu** though since only the virtual NTO of the T_1 amplitudes has significant similarity to the NTO for the $S_0 \rightarrow S_1$ transition (Table 6), while its character remains constant over the full range of $f(\epsilon_r)$ (Table S14).

For the model system **P1-NH2**, obtained via substitution of the CH_3 groups at the amino group against H atoms, the methodical error of CC2 (3.129 eV) compared to CC3 (3.169 eV) excitation energies is found to be 0.04 eV in vacuum (Table S10). For **P1** itself, CC3 (3.006 eV) reveals a slightly larger CC2 error of ∼0.08 eV (Table S11). Still, the better agreement with CC3 for CC2 than for ADC(2) indicates that CC2 is again more reliable here. As above for **N1-tBu**, the NTOs have been used to ensure that the same electronic states are involved.

Although the change in dipole moment upon excitation, $\Delta\mu = \mu(S_1) - \mu(S_0)$, is in vacuum larger for **P1** ($\Delta\mu \sim 10.5$ D) compared to **N1-tBu** ($\Delta\mu \sim -3.5$ D) and could indicate a larger change in the electronic structure, the discrepancy between ADC(2) and CC2 is smaller for **P1** compared to **N1-tBu**. This can probably be attributed to the larger $S_0 \rightarrow S_1$ gap in **P1** that counteracts the configuration mixing.

4.3. Additional Examples. Stimulated by these findings, we reanalyzed the results from the two previous benchmark studies by Winter et al.,[10,16] now with a focus on the difference between ADC(2) and CC2 (Table 7). For a set of 66 0−0 transition energies, a CC2−ADC(2) difference of (0.03 ± 0.06) eV (mean error ± standard deviation) was found, with only five cases exceeding a window of 0.1 eV.[10] Of these five, the three cases

https://doi.org/10.1021/acs.jctc.3c01355
J. Chem. Theory Comput. XXXX, XXX, XXX−XXX

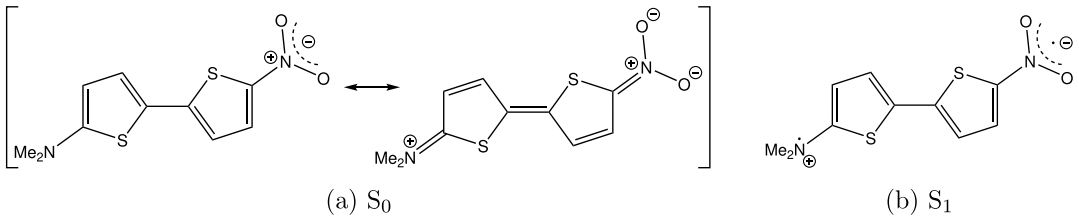


Figure 4. Lewis resonance structures of **P1** contributing to its singlet ground state (a) and first excited state (b).

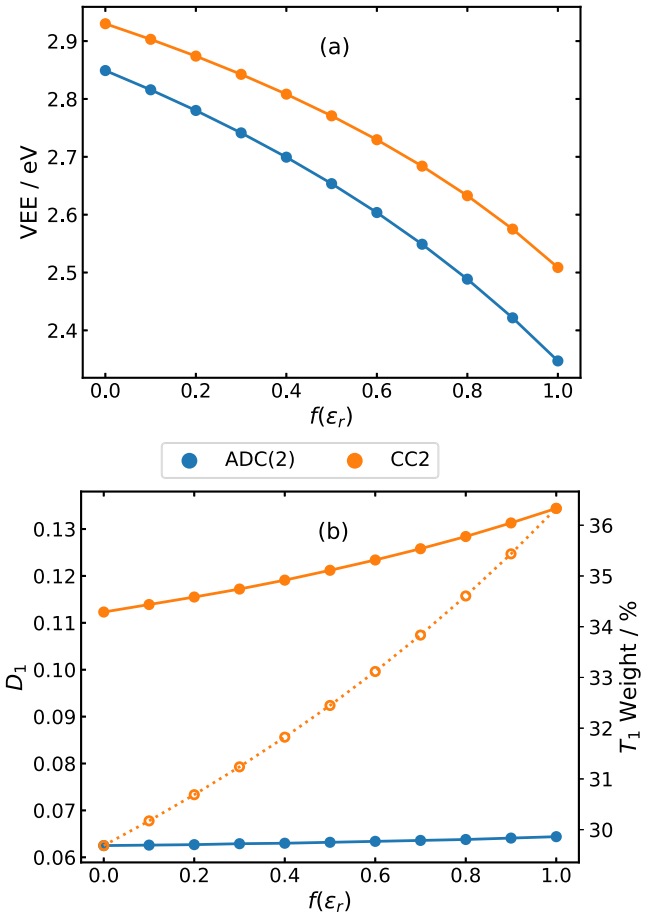


Figure 5. Variation of the ADC(2) and CC2 first vertical excitation energies in (a) and D_1 diagnostic values (solid lines, dots) and ground-state T_1 amplitude NTO weights (dashed lines, circles) in (b) with electric permittivity for **P1** in vacuum.

with the largest deviations are all $S_0 \rightarrow S_1$ transitions to totally symmetric S_1 states: porphycene (0.32 eV), 2-pyridone (0.24 eV), and salicylic acid (0.17 eV). For these three cases, ADC(2) significantly underestimates the experimental results, whereas in the other two cases involving nontotally symmetric states, ADC(2) is closer to the experiments (see ref 10 and references cited therein). Restricting to vertical transitions here, the difference between CC2 and ADC(2) reduces by a factor of 2−3, remaining above 0.1 eV only for porphycene and 2-pyridone (Table S15).

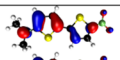
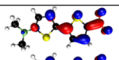
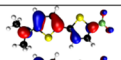
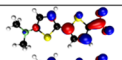
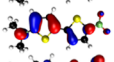
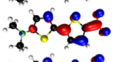
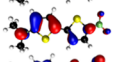
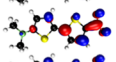
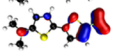
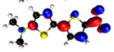
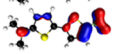
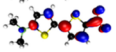
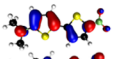
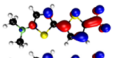
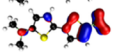
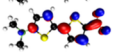
In another benchmark that investigates 89 vertical singlet excitations, a deviation of (0.02 ± 0.07) eV was found between the scaled opposite spin (SOS) variants SOS-CC2 and SOS-ADC(2).[16] Although the number of totally symmetric states in this set of vertical transitions is rather small and their energy is relatively high, also the largest CC2−ADC(2) difference is found for such a state: 0.22 eV for 2^1A_1, i.e., the lowest-lying $\pi\pi^*$ state of formaldehyde. Moderate differences were also observed for formamide (0.12 eV) and s-triazine (0.10 eV). Interestingly, using the nonscaled variants of ADC(2) and CC2, these differences are found to be even larger (Table S16): 0.23 eV (formaldehyde), 0.19 eV (formamide), and 0.15 eV (s-triazine). It should be noted here that the ADC(2) result for the $2^1A'$ state of formamide refers to an excitation energy averaged over S_3 and S_4 due to heavy mixing between the target $\pi \rightarrow \pi^*$ and another $\pi \rightarrow$ Rydberg state with almost equal contributions (Table S17). A similar observation is made for the 2^1A_1 state of formaldehyde (e.g., compare with ref 75) but also occurring for CC2, in addition to a different ordering of the corresponding states between ADC(2) and CC2 (Table S18). However, based on the NTOs, oscillator strengths, and a further comparison with CC3, the target $\pi\pi^*$ state could be identified.

In all cases in which CC2 and ADC(2) differ by more than 0.1 eV (i.e., except for salicylic acid), significant contributions from the T_1 amplitudes to these single excitations could be identified by referring to the NTOs (Tables S15 and S16). The dominant NTO pair for the T_1 amplitudes and those for the vertical electronic excitation are almost identical for formaldehyde (with a dominant T_1 NTO weight of ca. 58%) and s-triazine (2 × 32%; two degenerate NTO pairs) and very similar for formamide (55%), 2-pyridone (38%), and porphycene (27%). For porphycene, also contributions from the closely lying second excited state ($3^1A'$) could be identified in the second NTO pair for the T_1 amplitudes. Salicylic acid shows much less similarity between the NTOs (Table S16), in accordance with the rather low deviation for the vertical excitation energies. In this case, the difference between the ADC(2) and CC2 results for the 0−0 transition energies originates mainly from differences in the excited-state structure and zero vibrational energies.

It is an interesting observation that the selected examples from the second benchmark discussed here have turned out to be very convincing, additional cases for illustrating the role of singles amplitudes for totally symmetric states despite the fact that their excitation energies are already quite high and the deviation between ADC(2) and CC2 is typically expected to become less crucial with increasing excitation energy. Additional examples are the acid and base forms of tris(1,1,1,3,3,3-hexafluoropropan-2-yl)-8-hydroxypyrene-1,3,6-trisulfonate, in the following denoted as photoacid **B**, which have exhibited the largest deviations between ADC(2) and CC2 in two previous studies on hydroxypyrene-based photoacids.[28,29] As can be seen in Table 7, ADC(2) yields in the aug-cc-pVTZ basis set results that are 0.09 and 0.19 eV smaller than CC2 for the acid and base, respectively. In agreement with the twice as high deviation for the base of photoacid **B**, NTO analysis (Table S19) reveals fairly large singles contributions for the base—although the dominant NTO weight is quite low (9%)—and relatively smaller contributions for the acid.

https://doi.org/10.1021/acs.jctc.3c01355
J. Chem. Theory Comput. XXXX, XXX, XXX−XXX

Table 6. Overview on the Dominating NTO Pair for the First Electronic Transition with ADC(2), CC2, and CC3 as Well as for the CC2 Ground-State Singles Amplitudes of Dye P1 in Vacuum (Left) and in the Conductor Limit (Right)[a]

		Vacuum			Conductor Limit		
Method	State	Occ. NTO	Vir. NTO	Weight (D_1)	Occ. NTO	Vir. NTO	Weight (D_1)
ADC(2)	S_1			96.7 %			97.4 %
CC2	S_1			96.4 %			97.2 %
CC2	S_0			29.7 % (0.11)			36.3 % (0.13)
CC3	S_1			95.7 %	—	—	—
CC3	S_0			30.6 % (0.09)	—	—	—

[a]NTO weights and D_1 diagnostics are also included.

Table 7. Vertical Vacuum Electronic Excitation Energies with ADC(2) and CC2 in the aug-cc-pVTZ Basis Set[63,64] for Additional Examples

		calc. VEE/eV		difference/eV	
molecule	state[a]	ADC(2)	CC2	calc	lit.
porphycene[b]	$2^1A'$	2.105	2.237	0.132	0.320[c]
2-pyridone[b]	$2^1A'$	4.280	4.392	0.112	0.242[c]
salicylic acid[b]	$2^1A'$	4.241	4.298	0.057	0.169[c]
formaldehyde[d]	2^1A_1	~9.464[e,f]	~9.695[e,g]	0.231	0.22[h]
formamide[d]	$2^1A'$	~7.275[e,i]	7.461	0.186	0.12[h]
s-triazine[d]	$2^1A_1'$	7.109	7.255	0.146	0.10[h]
photoacid **B** (acid)[j]	2^1A	2.932	3.018	0.086	0.082[k]
photoacid **B** (base)[j]	2^1A	2.074	2.260	0.186	0.185[k]

[a]Labels acc. to ref 13. [b]B3-LYP/def2-TZVP geometries. [c]For 0−0 transition energies, taken from ref 10. [d]MP2/6-31G* geometries from ref 16 (as in refs 13−15). [e]Estimation needed due to state mixing. [f]S_2: 54% $\pi\pi^*$, 44% Rydberg; S_3: 31% $\pi\pi^*$, 68% Rydberg. [g]S_2: 25% $\pi\pi^*$, 74% Rydberg; S_3: 58% $\pi\pi^*$, 41% Rydberg. [h]For SOS vertical transition energies, taken from ref 16. [i]S_3: 42% $\pi\pi^*$, 57% Rydberg; S_4: 46% $\pi\pi^*$, 53% Rydberg. [j]Photoacid **B**: tris(1,1,1,3,3,3-hexafluoropropan-2-yl)-8-hydroxypyrene-1,3,6-trisulfonate; at CC2/cc-pVDZ geometries from ref 29. [k]For VEEs in aug-cc-pVDZ basis set, taken from ref 29.

5. CONCLUSIONS

This work has investigated the role of singles amplitudes for low-lying totally symmetric electronically excited states, which can cause significant deviations between the excitation energies calculated with the second-order methods ADC(2) and CC2, as demonstrated here with the examples of **N1-tBu** and **P1**. The opposite solvatochromism of these two dyes in combination with the implicit solvent model COSMO has allowed us to study the behavior of ADC(2) and CC2 in the limits of both very small and somewhat larger excitation energies by adjusting the $S_0 \rightarrow S_1$ transition energy through the solvent polarity (i.e., the dielectric constant). In addition, comparison with CC3 reference calculations have been used to address the accuracy of ADC(2) and CC2 in these situations.

The largest deviation between ADC(2) and CC2 has been observed for **N1-tBu** in vacuum, amounting to 0.45 eV. Analysis of the electronic transitions and singles amplitudes in terms of NTOs has revealed that the ground (S_0) and the first excited (S_1) state show a significant mixing of their leading configurations. Since ADC(2) uses by construction first-order MPPT amplitudes, ground-state singles are not included, in contrast to CC2 where they do contribute, giving rise to these deviations.

Despite the agreement with Plenert et al. regarding the deviation between ADC(2) and CC2 for **N1-tBu**, it appears that—in contrast to the conclusions drawn in ref 30—CC2 does indeed yield a qualitatively correct excitation energy in vacuum. In particular, the CC3-based theoretical best estimate (TBE) presented here demonstrates that an extrapolation of excitation energies measured in different environments, including rare gas matrices, via a polarity function can cause significant deviations with respect to the true vacuum result. Moreover, a comparison of geometries optimized using different methods—as part of the calculations for the TBE—also provides a nice example illustrating that MP2 and CC2 can yield geometries that can significantly differ (e.g., when probed by excitation energies).

For the negatively solvatochromic **N1-tBu**, the mixing between the leading configurations for S_0 and S_1 decreases with increasing polarity due to the increasing energy gap, i.e., the deviation of ADC(2) from CC2 becomes less severe for higher excitation energies. For the positively solvatochromic **P1**, the effects are much smaller than those for **N1-tBu**. The configuration mixing is rather small in vacuum and intensifies only moderately with solvent polarity, which is in line with smaller CC2−ADC(2) deviations for larger excitation energies. As such, these weaker effects are not related to the different type of solvatochromism on its own but rather to the smaller solvatochromic window in combination with less overlap between the NTOs of the ground-state singles with those for the $S_0 \rightarrow S_1$ transition. In vacuum, CC3 has been found to be closer to CC2 than to ADC(2) for both **P1** (higher excitation energy: ~3 eV) and **N1-tBu** (lower excitation energy: ~2 eV), indicating that CC2 performs better when the ground state shows significant mixing with singly excited configurations.

Although small $S_0 \rightarrow S_n$ gaps do facilitate a configuration mixing with the ground state, one cannot draw the conclusion that higher-lying valence-to-valence transitions are in general not affected. Reexamination of previous benchmarks[10,16] reveals that simple, small molecules like formaldehyde or formamide with significantly higher excitation energies compared to the two dyes studied here equally well exhibit significant contributions from the lowest-lying totally symmetric singly excited configurations to the ground state wavefunction. Of course, this relation is also still valid for the larger molecules among

https://doi.org/10.1021/acs.jctc.3c01355
J. Chem. Theory Comput. XXXX, XXX, XXX−XXX

them, e.g., s-triazine or the highly conjugated porphycene. Another interesting example with substantial deviations between ADC(2) and CC2 is photoacid **B** from ref 29.

Due to its Hermitian structure and the simplicity of the first-order ground-state wave function, ADC(2) provides often a useful alternative to CC2 for the exploration of excited-state potential energy surfaces. However, when the D_1(MP2) diagnostic indicates sizable contributions from singly excited configurations to the ground state, larger errors have to be expected for totally symmetric excited states when their transition vectors or the respective NTOs overlap with those for the ground state. For the examples studied in the current work, the comparison with CC3 results indicates that CC2 is more robust against such configuration mixing.

A sizable value for the D_1 diagnostic is a necessary but not a sufficient criterion for predicting deviations between ADC(2) and CC2 caused by ground-state singles contributions to the totally symmetric excited states (cf. Table 8). Seeking further for a simple criterion that correlates with the ADC(2)−CC2 deviation and also directly takes into account information on the excited state, we tested the overlap integral between the singles part of the excitation vector and the ground-state singles amplitudes (Table 8). Unfortunately, the correlation between the overlap $\langle R_1|T_1\rangle$ and the ADC(2)−CC2 difference (ΔE) is not very strong. Although the most extreme case, **N1-tBu** does show the largest overlap for both ADC(2) and CC2, the ordering of the examples in ΔE is not systematically reflected by the overlap. Therefore, we only feel confident enough to comment on the following two cases. If the $\langle R_1|T_1\rangle$ criterion for ADC(2) is

1. >0.01: moderate, but higher-than-average deviations
2. >0.03: extremely large deviations

between CC2 and ADC(2) are anticipated. However, there are outliers in both directions, as the T_1 amplitudes eventually affect all states for CC2.

In summary, we recommend that whenever the D_1(MP2) diagnostic indicates a significant configuration interaction between the ground and singly excited states,[71] the ADC(2) results for low-lying totally symmetric excited states should be used with caution. The $\langle R_1|T_1\rangle$ overlap and graphical inspection of the NTOs for these singles amplitudes provide an indication which states might be affected most. CC2 seems to be in some of these critical cases more robust although one should keep in mind that it is also a second-order single-reference method that will eventually fail if configuration interactions between the ground and excited states become too strong.[76]

Table 8. Comparison of the D_1 Diagnostic and the Overlap $\langle R_1|T_1\rangle$ between the Singles Parts of the Excitation Vectors (R_1) and the Ground-State Singles Amplitudes (T_1) as Potential Criteria for the ADC(2)−CC2 Deviation[d]

	ΔE[a,b]	$\langle R_1\|T_1\rangle$[b]		D_1[b]	
molecule	[eV]	ADC(2)	CC2	MP2	CC2
N1-tBu (C_{2v})	0.47	0.0543	0.1420	0.070	0.192
N1-tBu (C_2)	0.45	0.0543	0.0945	0.069	0.171
formaldehyde	0.23[c]	0.0115[c]	0.0151[c]	0.035	0.051
formamide	0.19[c]	0.0051[c]	0.0079	0.042	0.065
B (base)	0.16	0.0005	0.0171	0.065	0.123
triazine	0.15	0.0376	0.0645	0.038	0.063
porphycene	0.13	0.0361	0.0927	0.052	0.106
2-pyridone	0.11	0.0004	0.0040	0.045	0.073
B (acid)	0.08	0.0069	0.0165	0.058	0.110
P1	0.08	0.0067	0.0156	0.063	0.112
salicylic acid	0.06	0.0012	0.0033	0.049	0.081

[a]Difference between CC2 and ADC(2) excitation energies. [b]In the aug-cc-pVTZ basis set. [c]Estimated based on an average due to state mixing. [d](For the definition of $\langle R_1|T_1\rangle$ see the Supporting Information).

ASSOCIATED CONTENT

Supporting Information

The Supporting Information is available free of charge at https://pubs.acs.org/doi/10.1021/acs.jctc.3c01355.

Variation of the oscillator strength and excitation energy with the dielectric scaling function; variation of the vacuum-like and LR contributions to the excitation energy with the optical scaling function; evolution of the NTOs with the dielectric scaling function; NTO comparison between CC2 and CC3 (also model systems); comparison of twisted and planar geometries and composition of a TBE for the vacuum excitation energy; and NTO analysis for electronic transitions and singles amplitudes (PDF)

AUTHOR INFORMATION

Corresponding Author

Niklas Sülzner − *Lehrstuhl für Theoretische Chemie, Ruhr-Universität Bochum, 44780 Bochum, Germany;* orcid.org/0000-0002-8734-5807; Phone: +49 (0)234 32-24250; Email: niklas.suelzner@rub.de; Fax: +49 (0)234 32-14145

Author

Christof Hättig − *Lehrstuhl für Theoretische Chemie, Ruhr-Universität Bochum, 44780 Bochum, Germany;* orcid.org/0000-0002-5752-2710

Complete contact information is available at: https://pubs.acs.org/10.1021/acs.jctc.3c01355

Notes

The authors declare no competing financial interest.

ACKNOWLEDGMENTS

Funded by the Deutsche Forschungsgemeinschaft (DFG, German Research Foundation) under Germany's Excellence Strategy−EXC 2033−390677874−RESOLV.

REFERENCES

(1) Christiansen, O.; Koch, H.; Jørgensen, P. The second-order approximate coupled cluster singles and doubles model CC2. *Chem. Phys. Lett.* **1995**, *243*, 409−418.

(2) Schirmer, J. Beyond the random phase approximation: A new approximation scheme for the polarization propagator. *Phys. Rev. A* **1982**, *26*, 2395−2416.

(3) Loos, P.-F.; Scemama, A.; Jacquemin, D. The Quest for Highly Accurate Excitation Energies: A Computational Perspective. *J. Phys. Chem. Lett.* **2020**, *11*, 2374−2383.

(4) Hättig, C. In *Advances in Quantum Chemistry*; Jensen, H. J. A., Ed.; Response Theory and Molecular Properties (A Tribute to Jan Linderberg and Poul Jørgensen); Academic Press, 2005; Vol. *50*, pp 37−60.

(5) Jacquemin, D. What is the Key for Accurate Absorption and Emission Calculations, Energy or Geometry? *J. Chem. Theory Comput.* **2018**, *14*, 1534−1543.

https://doi.org/10.1021/acs.jctc.3c01355
J. Chem. Theory Comput. XXXX, XXX, XXX−XXX

(6) Loos, P.-F.; Jacquemin, D. Chemically Accurate 0−0 Energies with Not-so-Accurate Excited State Geometries. *J. Chem. Theory Comput.* **2019**, *15*, 2481−2491.
(7) Véril, M.; Scemama, A.; Caffarel, M.; Lipparini, F.; Boggio-Pasqua, M.; Jacquemin, D.; Loos, P.-F. QUESTDB: A database of highly accurate excitation energies for the electronic structure community. *Wiley Interdiscip. Rev. Comput. Mol. Sci.* **2021**, *11*, No. e1517.
(8) Loos, P.-F.; Jacquemin, D. Evaluating 0−0 Energies with Theoretical Tools: A Short Review. *ChemPhotoChem* **2019**, *3*, 684−696.
(9) Send, R.; Kühn, M.; Furche, F. Assessing Excited State Methods by Adiabatic Excitation Energies. *J. Chem. Theory Comput.* **2011**, *7*, 2376−2386.
(10) Winter, N. O. C.; Graf, N. K.; Leutwyler, S.; Hättig, C. Benchmarks for 0−0 transitions of aromatic organic molecules: DFT/B3LYP, ADC(2), CC2, SOS-CC2 and SCS-CC2 compared to high-resolution gas-phase data. *Phys. Chem. Chem. Phys.* **2013**, *15*, 6623−6630.
(11) Jacquemin, D.; Duchemin, I.; Blase, X. 0−0 Energies Using Hybrid Schemes: Benchmarks of TD-DFT, CIS(D), ADC(2), CC2, and BSE/GW formalisms for 80 Real-Life Compounds. *J. Chem. Theory Comput.* **2015**, *11*, 5340−5359.
(12) Suellen, C.; Freitas, R. G.; Loos, P.-F.; Jacquemin, D. Cross-Comparisons between Experiment, TD-DFT, CC, and ADC for Transition Energies. *J. Chem. Theory Comput.* **2019**, *15*, 4581−4590.
(13) Schreiber, M.; Silva-Junior, M. R.; Sauer, S. P. A.; Thiel, W. Benchmarks for electronically excited states: CASPT2, CC2, CCSD, and CC3. *J. Chem. Phys.* **2008**, *128*, 134110.
(14) Sauer, S. P. A.; Schreiber, M.; Silva-Junior, M. R.; Thiel, W. Benchmarks for Electronically Excited States: A Comparison of Noniterative and Iterative Triples Corrections in Linear Response Coupled Cluster Methods: CCSDR(3) versus CC3. *J. Chem. Theory Comput.* **2009**, *5*, 555−564.
(15) Silva-Junior, M. R.; Sauer, S. P.; Schreiber, M.; Thiel, W. Basis set effects on coupled cluster benchmarks of electronically excited states: CC3, CCSDR(3) and CC2. *Mol. Phys.* **2010**, *108*, 453−465.
(16) Winter, N. O. C.; Hättig, C. Scaled opposite-spin CC2 for ground and excited states with fourth order scaling computational costs. *J. Chem. Phys.* **2011**, *134*, 184101.
(17) Harbach, P. H. P.; Wormit, M.; Dreuw, A. The third-order algebraic diagrammatic construction method (ADC(3)) for the polarization propagator for closed-shell molecules: Efficient implementation and benchmarking. *J. Chem. Phys.* **2014**, *141*, 064113.
(18) Loos, P.-F.; Scemama, A.; Blondel, A.; Garniron, Y.; Caffarel, M.; Jacquemin, D. A Mountaineering Strategy to Excited States: Highly Accurate Reference Energies and Benchmarks. *J. Chem. Theory Comput.* **2018**, *14*, 4360−4379.
(19) Loos, P.-F.; Lipparini, F.; Boggio-Pasqua, M.; Scemama, A.; Jacquemin, D. A Mountaineering Strategy to Excited States: Highly Accurate Energies and Benchmarks for Medium Sized Molecules. *J. Chem. Theory Comput.* **2020**, *16*, 1711−1741.
(20) Loos, P.-F.; Scemama, A.; Boggio-Pasqua, M.; Jacquemin, D. Mountaineering Strategy to Excited States: Highly Accurate Energies and Benchmarks for Exotic Molecules and Radicals. *J. Chem. Theory Comput.* **2020**, *16*, 3720−3736.
(21) Loos, P.-F.; Jacquemin, D. A Mountaineering Strategy to Excited States: Highly Accurate Energies and Benchmarks for Bicyclic Systems. *J. Phys. Chem. A* **2021**, *125*, 10174−10188.
(22) Sarkar, R.; Boggio-Pasqua, M.; Loos, P.-F.; Jacquemin, D. Benchmarking TD-DFT and Wave Function Methods for Oscillator Strengths and Excited-State Dipole Moments. *J. Chem. Theory Comput.* **2021**, *17*, 1117−1132.
(23) Koch, H.; Christiansen, O.; Jørgensen, P.; Sanchez de Merás, A. M.; Helgaker, T. The CC3 model: An iterative coupled cluster approach including connected triples. *J. Chem. Phys.* **1997**, *106*, 1808−1818.
(24) Jacquemin, D.; Wathelet, V.; Perpète, E. A.; Adamo, C. Extensive TD-DFT Benchmark: Singlet-Excited States of Organic Molecules. *J. Chem. Theory Comput.* **2009**, *5*, 2420−2435.
(25) Christiansen, O.; Koch, H.; Jørgensen, P. Response functions in the CC3 iterative triple excitation model. *J. Chem. Phys.* **1995**, *103*, 7429−7441.
(26) Rückert, M. Implementation of COSMO- & PE-PNO-CC2 and their Application to Organic Molecules. M.Sc. Thesis; Ruhr-Universität Bochum: Bochum, Germany, 2019.
(27) Reichardt, C. Solvatochromic Dyes as Solvent Polarity Indicators. *Chem. Rev.* **1994**, *94*, 2319−2358.
(28) Sülzner, N.; Hättig, C. Theoretical Study on the Photoacidity of Hydroxypyrene Derivatives in DMSO Using ADC(2) and CC2. *J. Phys. Chem. A* **2022**, *126*, 5911−5923.
(29) Sülzner, N.; Hättig, C. Computational investigation of explicit solvent effects and specific interactions of hydroxypyrene photoacids in acetone, DMSO, and water. *Phys. Chem. Chem. Phys.* **2023**, *25*, 11130−11144.
(30) Plenert, A. C.; Mendez-Vega, E.; Sander, W. Micro- vs Macrosolvation in Reichardt's Dyes. *J. Am. Chem. Soc.* **2021**, *143*, 13156−13166.
(31) Christiansen, O. Coupled Cluster Theory with Emphasis on Selected New Developments. *Theor. Chim. Acta* **2006**, *116*, 106−123.
(32) Bartlett, R. J.; Musiał, M. Coupled-cluster theory in quantum chemistry. *Rev. Mod. Phys.* **2007**, *79*, 291−352.
(33) Bartlett, R. J. Coupled-cluster theory and its equation-of-motion extensions. *Wiley Interdiscip. Rev. Comput. Mol. Sci.* **2012**, *2*, 126−138.
(34) Sneskov, K.; Christiansen, O. Excited state coupled cluster methods. *Wiley Interdiscip. Rev. Comput. Mol. Sci.* **2012**, *2*, 566−584.
(35) Hald, K.; Jørgensen, P.; Olsen, J.; Jaszuński, M. An analysis and implementation of a general coupled cluster approach to excitation energies with application to the B2 molecule. *J. Chem. Phys.* **2001**, *115*, 671−679.
(36) Head-Gordon, M.; Oumi, M.; Maurice, D. Quasidegenerate second-order perturbation corrections to single-excitation configuration interaction. *Mol. Phys.* **1999**, *96*, 593−602.
(37) Helgaker, T.; Jørgensen, P.; Olsen, J. *Molecular Electronic-Structure Theory*; John Wiley & Sons: New York, 2000.
(38) Effenberger, F.; Würthner, F. 5-Dimethylamino-5′-nitro-2,2′-bithiophen - ein neuer Farbstoff mit ausgeprägter positiver Solvatochromie. *Angew. Chem.* **1993**, *105*, 742−744.
(39) Effenberger, F.; Wuerthner, F.; Steybe, F. Synthesis and Solvatochromic Properties of Donor-Acceptor-Substituted Oligothiophenes. *J. Org. Chem.* **1995**, *60*, 2082−2091.
(40) Klamt, A.; Schüürmann, G. COSMO: a new approach to dielectric screening in solvents with explicit expressions for the screening energy and its gradient. *J. Chem. Soc., Perkin Trans. 2* **1993**, 799−805.
(41) Schäfer, A.; Klamt, A.; Sattel, D.; Lohrenz, J. C. W.; Eckert, F. COSMO Implementation in TURBOMOLE: Extension of an efficient quantum chemical code towards liquid systems. *Phys. Chem. Chem. Phys.* **2000**, *2*, 2187−2193.
(42) Klamt, A. The COSMO and COSMO-RS solvation models. *Wiley Interdiscip. Rev. Comput. Mol. Sci.* **2011**, *1*, 699−709.
(43) Herbert, J. M. Dielectric continuum methods for quantum chemistry. *Wiley Interdiscip. Rev. Comput. Mol. Sci.* **2021**, *11*, No. e1519.
(44) Cossi, M.; Rega, N.; Scalmani, G.; Barone, V. Energies, structures, and electronic properties of molecules in solution with the C-PCM solvation model. *J. Comput. Chem.* **2003**, *24*, 669−681.
(45) Tapia, O.; Goscinski, O. Self-consistent reaction field theory of solvent effects. *Mol. Phys.* **1975**, *29*, 1653−1661.
(46) Christiansen, O.; Mikkelsen, K. V. A coupled-cluster solvent reaction field method. *J. Chem. Phys.* **1999**, *110*, 1365−1375.
(47) Christiansen, O.; Mikkelsen, K. V. Coupled cluster response theory for solvated molecules in equilibrium and nonequilibrium solvation. *J. Chem. Phys.* **1999**, *110*, 8348−8360.
(48) Aguilar, M. A.; del Valle, F. J. O.; Tomasi, J. Electron correlation and solvation effects. II. The description of the vibrational properties of a water molecule in a dielectric given by the application of the polarizable continuum model with inclusion of correlation effects. *Chem. Phys.* **1991**, *150*, 151−161.

https://doi.org/10.1021/acs.jctc.3c01355
J. Chem. Theory Comput. XXXX, XXX, XXX−XXX

(49) del Valle, F. J. O.; Tomasi, J. Electron correlation and solvation effects. I. Basic formulation and preliminary attempt to include the electron correlation in the quantum mechanical polarizable continuum model so as to study solvation phenomena. *Chem. Phys.* **1991**, *150*, 139−150.
(50) Schwabe, T.; Sneskov, K.; Olsen, J. M. H.; Kongsted, J.; Christiansen, O.; Hättig, C. PERI−CC2: A Polarizable Embedded RI-CC2 Method. *J. Chem. Theory Comput.* **2012**, *8*, 3274−3283.
(51) Khani, S. K.; Khah, A. M.; Hättig, C. COSMO-RI-ADC(2) excitation energies and excited state gradients. *Phys. Chem. Chem. Phys.* **2018**, *20*, 16354−16363.
(52) TURBOMOLE V7.7 2022, a development of University of Karlsruhe and Forschungszentrum Karlsruhe GmbH, 1989−2007, TURBOMOLE GmbH, 2007, available from https://www.turbomole.org.
(53) Franzke, Y. J.; Holzer, C.; Andersen, J. H.; Begušić, T.; Bruder, F.; Coriani, S.; Della Sala, F.; Fabiano, E.; Fedotov, D. A.; Fürst, S.; Gillhuber, S.; Grotjahn, R.; Kaupp, M.; Kehry, M.; Krstić, M.; Mack, F.; Majumdar, S.; Nguyen, B. D.; Parker, S. M.; Pauly, F.; Pausch, A.; Perlt, E.; Phun, G. S.; Rajabi, A.; Rappoport, D.; Samal, B.; Schrader, T.; Sharma, M.; Tapavicza, E.; Treß, R. S.; Voora, V.; Wodyński, A.; Yu, J. M.; Zerulla, B.; Furche, F.; Hättig, C.; Sierka, M.; Tew, D. P.; Weigend, F. TURBOMOLE: Today and Tomorrow. *J. Chem. Theory Comput.* **2023**, *19*, 6859−6890.
(54) TURBOMOLE V7−7-454-g07a3bc24e5; a development of University of Karlsruhe and Forschungszentrum Karlsruhe GmbH, 1989-2007, TURBOMOLE GmbH, 2007, available from https://www.turbomole.org.
(55) Eichkorn, K.; Treutler, O.; Öhm, H.; Häser, M.; Ahlrichs, R. Auxiliary basis sets to approximate Coulomb potentials. *Chem. Phys. Lett.* **1995**, *240*, 283−290.
(56) Eichkorn, K.; Weigend, F.; Treutler, O.; Ahlrichs, R. Auxiliary basis sets for main row atoms and transition metals and their use to approximate Coulomb potentials. *Theor. Chim. Acta* **1997**, *97*, 119−124.
(57) Sülzner, N.; Hättig, C. *Raw Data to "Role of Singles Amplitudes in ADC(2) and CC2 for Low-Lying Electronically Excited States. Zenodo*, 2023, DOI: 10.5281/zenodo.10256897.
(58) Becke, A. D. Density-functional exchange-energy approximation with correct asymptotic behavior. *Phys. Rev. A* **1988**, *38*, 3098−3100.
(59) Lee, C.; Yang, W.; Parr, R. G. Development of the Colle-Salvetti correlation-energy formula into a functional of the electron density. *Phys. Rev. B* **1988**, *37*, 785−789.
(60) Becke, A. D. Density-functional thermochemistry. III. The role of exact exchange. *J. Chem. Phys.* **1993**, *98*, 5648−5652.
(61) Treutler, O.; Ahlrichs, R. Efficient molecular numerical integration schemes. *J. Chem. Phys.* **1995**, *102*, 346−354.
(62) Weigend, F.; Ahlrichs, R. Balanced basis sets of split valence, triple zeta valence and quadruple zeta valence quality for H to Rn: Design and assessment of accuracy. *Phys. Chem. Chem. Phys.* **2005**, *7*, 3297−3305.
(63) Kendall, R. A.; Dunning, T. H.; Harrison, R. J. Electron affinities of the first-row atoms revisited. Systematic basis sets and wave functions. *J. Chem. Phys.* **1992**, *96*, 6796−6806.
(64) Woon, D. E.; Dunning, T. H. Gaussian basis sets for use in correlated molecular calculations. III. The atoms aluminum through argon. *J. Chem. Phys.* **1993**, *98*, 1358−1371.
(65) Hättig, C. Geometry optimizations with the coupled-cluster model CC2 using the resolution-of-the-identity approximation. *J. Chem. Phys.* **2003**, *118*, 7751−7761.
(66) Dunning, T. H. Gaussian basis sets for use in correlated molecular calculations. I. The atoms boron through neon and hydrogen. *J. Chem. Phys.* **1989**, *90*, 1007−1023.
(67) Woon, D. E.; Dunning, T. H., Jr. Gaussian basis sets for use in correlated molecular calculations. IV. Calculation of static electrical response properties. *J. Chem. Phys.* **1994**, *100*, 2975−2988.
(68) Amos, A. T.; Hall, G. G.; Jones, H. Single determinant wave functions. *Proc. R. Soc. London, A* **1961**, *263*, 483−493.
(69) Martin, R. L. Natural transition orbitals. *J. Chem. Phys.* **2003**, *118*, 4775−4777.
(70) Batista, E. R.; Martin, R. L. *Encyclopedia of Computational Chemistry*; John Wiley & Sons, Ltd, 2004.
(71) Janssen, C. L.; Nielsen, I. M. B. New diagnostics for coupled-cluster and Møller−Plesset perturbation theory. *Chem. Phys. Lett.* **1998**, *290*, 423−430.
(72) Send, R.; Kaila, V. R. I.; Sundholm, D. Reduction of the virtual space for coupled-cluster excitation energies of large molecules and embedded systems. *J. Chem. Phys.* **2011**, *134*, 214114.
(73) Reichardt, C. Pyridinium N-phenolate betaine dyes as empirical indicators of solvent polarity: Some new findings. *Pure Appl. Chem.* **2004**, *76*, 1903−1919.
(74) Bai, S.; Mansour, R.; Stojanović, L.; Toldo, J. M.; Barbatti, M. On the origin of the shift between vertical excitation and band maximum in molecular photoabsorption. *J. Mol. Model.* **2020**, *26*, 107−115.
(75) Mewes, S. A.; Plasser, F.; Krylov, A.; Dreuw, A. Benchmarking Excited-State Calculations Using Exciton Properties. *J. Chem. Theory Comput.* **2018**, *14*, 710−725.
(76) Pabst, M.; Köhn, A.; Gauss, J.; Stanton, J. F. A worrisome failure of the CC2 coupled-cluster method when applied to ozone. *Chem. Phys. Lett.* **2010**, *495*, 135−140.

https://doi.org/10.1021/acs.jctc.3c01355
J. Chem. Theory Comput. XXXX, XXX, XXX−XXX